

This discussion paper is/has been under review for the journal *Atmospheric Chemistry and Physics (ACP)*. Please refer to the corresponding final paper in *ACP* if available.

**Tracking volcanic  
SO<sub>2</sub> with IASI**

L. Clarisse et al.

# Tracking and quantifying volcanic SO<sub>2</sub> with IASI, the September 2007 eruption at Jebel at Tair

L. Clarisse<sup>1</sup>, P. F. Coheur<sup>1</sup>, A. J. Prata<sup>2</sup>, D. Hurtmans<sup>1</sup>, A. Razavi<sup>1</sup>, T. Phulpin<sup>3</sup>, J. Hadji-Lazaro<sup>4</sup>, and C. Clerbaux<sup>4,1</sup>

<sup>1</sup>Spectroscopie de l'Atmosphère, Service de Chimie Quantitative Photophysique, Université Libre de Bruxelles, Brussels, Belgium

<sup>2</sup>Norwegian Institute for Air Research, Kjeller, Norway

<sup>3</sup>Centre National d'Etudes Spatiales, 18 Avenue E. Belin, 31401 Toulouse, France

<sup>4</sup>UPMC Université Paris 06, CNRS UMR 7620, Service d'Aéronomie/IPSL, Paris, France

Received: 14 July 2008 – Accepted: 4 August 2008 – Published: 9 September 2008

Correspondence to: L. Clarisse (lclariss@ulb.ac.be)

Published by Copernicus Publications on behalf of the European Geosciences Union.

Title Page

Abstract

Introduction

Conclusions

References

Tables

Figures

◀

▶

◀

▶

Back

Close

Full Screen / Esc

Printer-friendly Version

Interactive Discussion



## Abstract

In this paper we demonstrate the potential of the infrared Fourier transform spectrometer IASI in analysing volcanic eruptions, using the September 2007 eruption at Jebel at Tair as an illustrative example. Detailed radiative transfer calculations are presented, simulating IASI-like transmittance spectra for a variety of volcanic plumes. We analyse the sensitivity of IASI to SO<sub>2</sub> at different altitudes and demonstrate that IASI is in principle capable of sensing SO<sub>2</sub> down to the surface. Using the brightness temperature difference of well chosen SO<sub>2</sub> channels as a filter, we are able to track the plume of the Jebel at Tair eruption for 12 days, on a par with state of the art UV sounders. A method is presented for quickly estimating the altitude of a volcanic plume based on the relative intensities of the SO<sub>2</sub> absorption lines. Despite recent advances, it is still very challenging to retrieve vertical profiles of SO<sub>2</sub> from nadir viewing satellites. Currently the most accurate profiles in nadir are retrieved using backtracking of the plume with atmospheric transport models. Via full inverse retrievals using the optimal estimation method, we show the possibility of extracting medium coarse vertical profiles from IASI data. The retrieval allows us to present an evolution of the total mass of SO<sub>2</sub> in the plume for the Jebel at Tair eruption. An analytical relation is derived between brightness temperature differences and concentrations, which fits the experimental data very well. The spectral range of IASI also allows retrieval of volcanic aerosols. In the initial plume of the Jebel at Tair eruption, volcanic aerosols were found in the form of ice particles, for which we derived particle sizes.

## 1 Introduction

Yearly, an estimated 5–20% of the total global sulphur emission is due to volcanic sulphur dioxide (Halmer et al., 2002). The impact of SO<sub>2</sub> on the atmosphere is very much dependent on the height of the eruption. In the troposphere, sulphur dioxide oxidises to sulphate after which it is washed out quickly. The lifetime of SO<sub>2</sub> in the

## Tracking volcanic SO<sub>2</sub> with IASI

L. Clarisse et al.

Title Page

Abstract

Introduction

Conclusions

References

Tables

Figures

◀

▶

◀

▶

Back

Close

Full Screen / Esc

Printer-friendly Version

Interactive Discussion



stratosphere is of the order of weeks, during which time it gradually forms sulphuric acid aerosols, which have a lifetime in the atmosphere of about three years. These aerosols have an important impact on the global climate as they increase the earth's albedo through scattering of sunlight. Quantifying natural SO<sub>2</sub> is crucial in comparing natural versus anthropogenic emissions and their respective impact on climate (Andres and Kasgnoc, 1998). Large eruptions also provide an opportunity to validate climate models because of the relatively short perturbation on the climate system (Robock, 2000). Apart from these long term interests, monitoring SO<sub>2</sub> has an application as a surrogate for tracking volcanic ash clouds for aviation hazards (Stunder et al., 2007).

Due to their spatial and temporal distribution, volcanic eruptions are best monitored from space. Currently there are quite a few remote sensing satellites capable of quantitative sensing of SO<sub>2</sub>. Spaceborne ozone monitors measure radiation using backscattered ultraviolet sunlight (BUV) and are often able to measure the SO<sub>2</sub> absorption feature at 230–330 nm. Examples include the Total Ozone Mapping Spectrometer (TOMS, e.g. Krueger et al., 1995), the Global Ozone Monitoring Experiment (GOME, e.g. Loyola et al., 2008) and more recently the Scanning Imaging Absorption Spectrometer for Atmospheric Cartography (SCIAMACHY, e.g. Lee et al., 2008) and Ozone Monitoring Instrument (OMI, e.g. Yang et al., 2007). Thanks to their large swath these BUV instruments on polar satellites can offer a rapid full coverage of the Earth but as they rely on daylight hours it is only obtained at best once a day. Satellite instruments that sound in the infrared do not have this limitation. For the detection of SO<sub>2</sub>, they rely on either the symmetric stretch  $\nu_1$  centred at 1152 cm<sup>-1</sup>, the antisymmetric stretch  $\nu_3$  centred at 1362 cm<sup>-1</sup> and possibly the weaker  $\nu_1 + \nu_3$  combination band at 2500 cm<sup>-1</sup>. Apart from SO<sub>2</sub>, IR sounders are generally also capable of quantifying volcanic aerosols, e.g. silicate ash and ice sometimes found in the initial plume. Moderate resolution infrared imagers such as the Moderate Resolution Imaging Spectroradiometer (MODIS, e.g. Watson et al., 2004) and the Spinning Enhanced Visible and InfraRed Imager (SEVIRI, e.g. Prata and Kerkmann, 2007) typically have a very good spatial and temporal resolution, but poor spectral resolution. Examples of high resolution IR sounders used to

**Tracking volcanic  
SO<sub>2</sub> with IASI**

L. Clarisse et al.

Title Page

Abstract

Introduction

Conclusions

References

Tables

Figures

◀

▶

◀

▶

Back

Close

Full Screen / Esc

Printer-friendly Version

Interactive Discussion



retrieve SO<sub>2</sub> include the Atmospheric Infrared Sounder (AIRS, e.g. Carn et al., 2005), the Tropospheric Emission Spectrometer (TES, e.g. Clerbaux et al., 2008<sup>1</sup>) and the Infrared Atmospheric Sounding Interferometer (IASI).

Recently, the September 2007 eruption of Jebel at Tair was analysed using AIRS, OMI, SEVIRI and lidar backscatter sounder CALIPSO data (Eckhardt et al., 2008). In this paper we demonstrate IASI's potential in analysing volcanic eruptions, using this eruption as an illustrative example.

## 2 IASI and the eruption on Jebel at Tair

The polar-orbiting MetOp-A was launched on 19 October 2006 and carries on board the Fourier transform spectrometer IASI (see Clerbaux et al., 2007; Phulpin et al., 2007 and <http://smc.cnes.fr/IASI/>). It provides global coverage twice a day in the nadir geometry (polar sun-synchronous), with a footprint of 12 km diameter and full swath width of 2200 km. MetOp is an operational platform, so that the measurements are available in near real time. The spectrometer has a spectral coverage from 645 cm<sup>-1</sup> to 2760 cm<sup>-1</sup> with no gaps, an apodized resolution of 0.5 cm<sup>-1</sup> and a spectral sampling of 0.25 cm<sup>-1</sup>. The instrument covers the  $\nu_1$ ,  $\nu_3$  and  $\nu_1 + \nu_3$  bands of SO<sub>2</sub> completely as well as volcanic ash and aerosol absorption features typical between 800 cm<sup>-1</sup> and 1300 cm<sup>-1</sup> (Wen and Rose, 1994). From on-flight analysis the Noise Equivalent Delta Temperature (NEDT) at 280 K is estimated to be 0.05 K in the  $\nu_3$  and 0.12 K in the  $\nu_1$  band, significantly better than the expected 0.2–0.35 K. These specifications also compare favourably to the AIRS instrument, which has an NEDT of about 0.2 K and only partially covers the  $\nu_1$  band (Carn et al., 2005).

<sup>1</sup>Clerbaux, C., Coheur, P.-F., Clarisse, L., Hadji-Lazaro, J., Hurtmans, D., Turquety, S., Bowman, K., Worden, H., and Carn, S.: Measurements of SO<sub>2</sub> profiles in volcanic plumes using the TES/AURA high-resolution infrared satellite observations, submitted, Geophys. Res. Lett., 2008.

Title Page

Abstract

Introduction

Conclusions

References

Tables

Figures

◀

▶

◀

▶

Back

Close

Full Screen / Esc

Printer-friendly Version

Interactive Discussion



Jebel at Tair is a stratovolcano located in the Red Sea between Yemen and Eritrea (15.54° N, 41.83° E), its last eruption dates back to 1883 (see <http://www.volcano.si.edu>). In the afternoon of 30 September 2007, the volcano violently erupted, killing several people from the Yemen military base on the island. The exact time of the eruption is not known, but it is estimated to have happened between 11:00 and 12:00 UTC (Eckhardt et al., 2008). The first view of the volcanic plume erupted by Jebel at Tair was caught by IASI at 30 September 2007 around 18:48 UTC (Fig. 1 and Fig. 8). The plume could be tracked for 12 days travelling more than 20 000 km, from Sudan, Egypt, Iraq, Iran, Afghanistan, China, Japan returning through the Philippine Sea, the Philippine Islands, Vietnam, Laos, Myanmar, Bangladesh and finally India (Fig. 2). This compares very well to BUV sounders such as OMI (<http://so2.umbc.edu/omi/pix/special/2007/redsea/altair07.php>).

### 3 Altitude information

In this section we outline some spectroscopic features of transmittance spectra relevant to the estimation of the altitude of a volcanic plume. We have simulated radiance spectra for a variety of plumes with different peak altitude and SO<sub>2</sub> concentration, in order to see their impact on the spectra. The calculations were carried out with the software Atmosphit, developed at the Université Libre de Bruxelles (<http://home.scarlet.be/dhurtma/atmosphit.html>). We start by summarizing the main features of Atmosphit's forward modelling. For the details we refer to Barret et al. (2005a,b), Coheur et al. (2005) and Rodgers (2000).

#### 3.1 Forward model

Dividing the atmosphere in different layers  $k$ , with assumed constant temperature  $T_k$ , pressure  $p_k$  and volume-mixing ratios, the upward radiance at wavenumber  $\nu$  entering

Title Page

Abstract

Introduction

Conclusions

References

Tables

Figures

◀

▶

◀

▶

Back

Close

Full Screen / Esc

Printer-friendly Version

Interactive Discussion



layer  $k+1$  can be approximated by

$$R_{k+1}(v) = R_k(v)\tau_k + B(v, T_k)(1 - \tau_k), \quad (1)$$

with  $\tau_k$  the effective transmittance of layer  $k$  and  $B(v, T)$  the Planck function of a blackbody at temperature  $T$  and wavenumber  $v$ . The radiance emitted by the surface is approximated by  $R_0 = \epsilon_s B(v, T_s) + R_r$ , with  $\epsilon_s$  the emissivity of the surface, and  $R_r$  the reflected downwelling flux. The first term in Eq. (1) represents the fraction of the radiance entering layer  $k$  which is transmitted through layer  $k+1$ . The second term represents the radiation emitted by layer  $k$ . This discrete radiative transfer equation assumes local thermodynamic equilibrium everywhere. To evaluate the radiance emitted at the top of the atmosphere, Eq. (1) is iteratively evaluated for every wavenumber within the range of interest. The effective transmittance is given by

$$\tau_k = \exp \left[ - \sum_i \Phi_i(\rho_k, T_k, n_{i,k}, v) C_{i,k} \right], \quad (2)$$

where the sum runs over different species  $i$ . Here the coefficients  $n_{i,k}$  denote average molecular number densities and  $C_{i,k}$  molecular partial columns. In the evaluation of the latter quantity, the effects of refraction are incorporated via ray tracing. The coefficients  $\Phi_i$  represent the discrete absorption line shape or continuous band shape specific to the species  $i$ . These are calculated using a Voigt line shape and the line parameters in the HITRAN database (Rothman et al., 2005). The absorption continua of water vapour, carbon dioxide, oxygen and nitrogen are incorporated using the MT\_CKD 1.03 model (Mlawer et al., 2003). Finally the Fourier transform infrared instrumental line-shape of IASI, including apodization and field of view, is taken into account.

### 3.2 Simulations and discussion

The atmospheric conditions were specified using a standard tropical model (15N latitude) defining average temperature, pressure and volume mixing ratios for 28 molecules in one kilometre thick layers from the ground up to sixty kilometre high. The

Title Page

Abstract

Introduction

Conclusions

References

Tables

Figures

◀

▶

◀

▶

Back

Close

Full Screen / Esc

Printer-friendly Version

Interactive Discussion



surface temperature was fixed at 300 K. For each simulation a different amount of SO<sub>2</sub> was inserted in a single 500 m thick layer located between 1 km and 30 km. Figure 3 shows the difference in brightness temperature (BT) between the baseline (300 K) and the three strongest absorption lines of the  $\nu_1$  and the  $\nu_3$  band as a function of the altitude of the SO<sub>2</sub> plume. The specific lines with the strongest absorption vary with altitude and concentration of the plume and give an accurate idea of the sensitivity of IASI. The four different curves represent different amounts of SO<sub>2</sub> in Dobson Units (1 DU equals  $2.69 \cdot 10^{16}$  molecules per cm<sup>2</sup>). Both bands have highest sensitivity between 16 and 18 km, which coincides with the cold point tropopause in the tropical model. The  $\nu_3$  band is clearly more sensitive than the  $\nu_1$ , except below 4 km. In the region 1300–1400 cm<sup>-1</sup> the water vapour in the atmosphere absorbs nearly all radiation coming from the ground. The atmosphere is only sufficiently transparent at a higher altitude, where the concentration of water vapour is lower (Prata and Bernardo, 2007). For a 100 DU SO<sub>2</sub> plume at 1 km altitude, the highest brightness temperature differences are 1 K in the  $\nu_1$  band and 0.7 K in the  $\nu_3$  band. IASI has an instrumental noise lower than 0.12 K and should be able to see this. IASI is therefore in principle capable of sensing SO<sub>2</sub> down to the ground, but much will depend on the precise atmospheric conditions such as the water vapour profile and the thermal contrast between the surface and the first atmospheric layer.

Figure 4 illustrates the impact of water vapour on the observed intensities. Figure 4a shows the pseudo transmittance spectra of an over-simplified atmosphere containing nothing but 100 DU of SO<sub>2</sub> (again at different altitudes). The only aspect really affecting the intensity of the lines is the thermal contrast between the source (surface) and the temperature of the SO<sub>2</sub> layer. Figure 4b shows the same pseudo transmittance spectra, but this time in an atmosphere populated with water vapour (and the other molecules from the standard model). As mentioned above, water vapour absorbs almost all radiation at low altitude, making the observation almost insensitive to SO<sub>2</sub> in the boundary layer. The spectra in Fig. 4 are pseudo transmittance spectra because they represent the ratio of an atmosphere with and without SO<sub>2</sub>. In contrast,

**Tracking volcanic  
SO<sub>2</sub> with IASI**

L. Clarisse et al.

[Title Page](#)[Abstract](#)[Introduction](#)[Conclusions](#)[References](#)[Tables](#)[Figures](#)[◀](#)[▶](#)[◀](#)[▶](#)[Back](#)[Close](#)[Full Screen / Esc](#)[Printer-friendly Version](#)[Interactive Discussion](#)

**Tracking volcanic  
SO<sub>2</sub> with IASI**

L. Clarisse et al.

Title Page

Abstract

Introduction

Conclusions

References

Tables

Figures

◀

▶

◀

▶

Back

Close

Full Screen / Esc

Printer-friendly Version

Interactive Discussion



the effective transmittance is only very weakly dependent on the altitude. To scan daily global data for exceptional concentrations of SO<sub>2</sub>, we have designed a BT difference filter which calculates BTs at four different IASI channels. The channels at  $\nu'_0=1407.25$  and  $\nu''_0=1408.75$  are used to estimate the baseline;  $\nu'_3=1371.50$  and  $\nu''_3=1371.75$  to estimate absorption in the  $\nu_3$  band. These channels were chosen so as to minimise false alerts caused by water vapour interference, while maximising sensitivity. On 30 September, BT differences as large as 50 K (for the  $\nu_3$  band) were measured in the plume from Jebel at Tair. In view of Fig. 3 this gives a lower bound of 80 DU on the concentration and puts the peak altitude immediately in the range 12–21 km. For this particular eruption this is already a reasonably good estimate. Absolute intensities for eruptions where the plume does not reach a high altitude will not give us any of this information, as the BT difference will be much smaller.

To quantify the plume's altitude, instead of looking at the absolute intensities, we can also look at the relative intensities of the absorption lines. As an example, Fig. 5 shows the ratio  $R(1347.25, 1368.00)$  between the pseudo transmittance coefficients in the IASI channels at  $1347.25\text{ cm}^{-1}$  and at  $1368.00\text{ cm}^{-1}$  in function of altitude and concentration. For large concentrations of SO<sub>2</sub> this ratio tells us whether the peak altitude is below or above 10 km. For the eruption at Jebel at Tair, typical pseudo transmittance spectra on 30 September have ratios between 1.4 and 1.5, putting the plume in the range 14–19 km with concentrations higher than 60 DU. Analogous results were obtained with other choices of channels for the ratio  $R$ . The pseudo transmittance spectra were calculated from the radiance spectra (the target spectra) through division by a reference spectrum. The reference spectra were chosen to have the same baseline as the target spectra and unaffected by SO<sub>2</sub>. They are typically found geographically close to the target (see also Prata and Bernardo, 2007). It is very important that the reference spectrum is chosen properly, as the ratio  $R$  can be quite sensitive to a bad choice. Looking at BT differences and intensity ratios is a quick way of estimating concentration and altitude of a volcanic plume. In the case of large volcanic eruptions, more accurate estimates can be obtained via inverse SO<sub>2</sub> profile retrievals, which we

will discuss in detail in the next section.

## 4 Full retrievals

### 4.1 Inverse model

As with the forward model, the inverse model was also carried out with the help of Atmosphit. Again, we will sketch the method and refer for details again to Barret et al. (2005a), Barret et al. (2005b) Coheur et al. (2005) and Rodgers (2000). Let us assume for the time being that the forward model is linear, i.e.

$$\mathbf{y} = \mathbf{K}\mathbf{x} + \boldsymbol{\epsilon},$$

with  $\mathbf{y}$  representing the measurement vector (the radiances) and  $\mathbf{x}$  representing the state vector (parameters we would like to retrieve such as surface temperature, and concentrations and constant model parameters such as the pressure and temperature profiles). The forward model is represented by the weighting function or kernel  $\mathbf{K}$ , the measurement error by  $\boldsymbol{\epsilon}$ .

This type of inverse problem is generally ill-posed, with no exact solution. There are a number of ways to find a regularized solution  $\hat{\mathbf{x}}$  which approximates the true state  $\mathbf{x}$ . The optimal estimation method presented in Rodgers (2000) uses a Bayesian approach. It combines the measurement result  $\mathbf{y}$  and its measurement covariance matrix  $\mathbf{S}_e$  with the a priori knowledge of the state  $\mathbf{x}_a$  and its covariance  $\mathbf{S}_a$  to yield a maximum a posteriori solution  $\hat{\mathbf{x}}$  with covariance  $\hat{\mathbf{S}}$ . The solution is given by (here we give the so-called  $n$ -form of the solution)

$$\hat{\mathbf{x}} = \mathbf{x}_a + (\mathbf{K}^T \mathbf{S}_e^{-1} \mathbf{K} + \mathbf{S}_a^{-1})^{-1} \mathbf{K}^T \mathbf{S}_e^{-1} (\mathbf{y} - \mathbf{K}\mathbf{x}_a) \quad (3)$$

and

$$\hat{\mathbf{S}}^{-1} = \mathbf{K}^T \mathbf{S}_e^{-1} \mathbf{K} + \mathbf{S}_a^{-1}.$$

## Tracking volcanic SO<sub>2</sub> with IASI

L. Clarisse et al.

Title Page

Abstract

Introduction

Conclusions

References

Tables

Figures

◀

▶

◀

▶

Back

Close

Full Screen / Esc

Printer-friendly Version

Interactive Discussion



Writing

$$\mathbf{K} = \frac{\partial \mathbf{y}}{\partial \mathbf{x}} \text{ and } \mathbf{G} = \frac{\partial \hat{\mathbf{x}}}{\partial \mathbf{y}},$$

with the gain matrix  $\mathbf{G} = (\mathbf{K}^T \mathbf{S}_e^{-1} \mathbf{K} + \mathbf{S}_a^{-1})^{-1} \mathbf{K}^T \mathbf{S}_e^{-1}$ , we can introduce the averaging kernel

$$\mathbf{A} = \mathbf{GK} = \frac{\partial \hat{\mathbf{x}}}{\partial \mathbf{x}}.$$

In words, the kernel is the sensitivity of the measurement to the real state, the gain matrix the sensitivity of the retrieved state to the measurement and the averaging kernel the sensitivity of the retrieved state to the true state. In the idealized case where the problem is well determined we have  $\hat{\mathbf{x}} = \mathbf{x} + \mathbf{K}^{-1} \boldsymbol{\epsilon}$  and  $\mathbf{A} = \mathbf{I}$ . More generally though, we can rewrite Eq. (3) as

$$\hat{\mathbf{x}} = \mathbf{Ax} + (\mathbf{I} - \mathbf{A})\mathbf{x}_a + \mathbf{G}\boldsymbol{\epsilon},$$

so that the retrieved state is the weighted average of the true state with the a priori state. The more  $\mathbf{A}$  resembles the identity matrix  $\mathbf{I}$ , the better  $\hat{\mathbf{x}}$  will resemble  $\mathbf{x}$ . The resemblance is commonly quantified by the trace of  $\mathbf{A}$  and goes under the name “degrees of freedom for signal” (DOFS). It gives an estimate on the number of retrieved independent pieces of information.

For a moderately non-linear problem like ours, we have  $\mathbf{y} = \mathbf{F}(\mathbf{x}) + \boldsymbol{\epsilon}$ . Via Newton methods, the solution of Eq. (4) can be approximated by the iterative solution

$$\hat{\mathbf{x}}_{i+1} = \mathbf{x}_a + (\mathbf{K}_i^T \mathbf{S}_e^{-1} \mathbf{K}_i + \mathbf{S}_a^{-1})^{-1} \mathbf{K}_i^T \mathbf{S}_e^{-1} (\mathbf{y} - \mathbf{F}(\hat{\mathbf{x}}_i) + \mathbf{K}(\hat{\mathbf{x}}_i - \mathbf{x}_a)), \quad (4)$$

where  $\mathbf{K} = \frac{\partial \mathbf{F}}{\partial \mathbf{x}}$  and  $\mathbf{K}_i = \mathbf{K}(\mathbf{x}_i)$ .

Tracking volcanic  
SO<sub>2</sub> with IASI

L. Clarisse et al.

Title Page

Abstract

Introduction

Conclusions

References

Tables

Figures

◀

▶

◀

▶

Back

Close

Full Screen / Esc

Printer-friendly Version

Interactive Discussion



## 4.2 Retrieval parameters

For the Jebel at Tair eruption we did not use the  $\nu_1$  band for the retrieval. The presence of an ice signature makes an accurate retrieval hard in this band (see Sect. 5). The band is also affected by emissivity features over arid land. The plume passed over both the Arabian desert and the Gobi desert, where the emissivity is strongly dependent on the wavenumber in the region  $800\text{--}1300\text{ cm}^{-1}$  (see e.g. Li et al., 2007). For the retrievals we considered therefore only the  $\nu_3$  absorption feature. The disadvantage of this band is the strong competition of water vapour absorption. An accurate retrieval of the vertical profile of water vapour is essential, and for this reason the fitting range was set to  $1310\text{--}1450\text{ cm}^{-1}$ . This range not only contains the complete  $\nu_3$  band of  $\text{SO}_2$ , but also contains a large part of the  $\nu_2$  band of  $\text{H}_2\text{O}$ . Other interfering molecules in this range include  $\text{CH}_4$  and  $\text{N}_2\text{O}$  and total columns were fitted for those. For water vapour, concentrations were retrieved in 1 km thick partial columns, from the surface up to 20 km. For the first 36 h after the eruption,  $\text{SO}_2$  was retrieved in three partial columns: 12–15 km, 15–18 km and 18–21 km. This choice was motivated by the analysis presented in Sect. 3. For spectra recorded after 1 October, one total column was fitted between 15–18 km (see Sect. 4.3.2). The spectra for the retrieval were selected on the basis of the BT difference between the  $\nu_3$  band and the baseline. Only spectra with a BT difference larger than 0.5 K were retained. A priori values for all molecules were taken from either the tropical or midlatitude summer model, and pressure and temperature profiles were interpolated from data from the ECMWF to match date and location of the IASI measurements. The measurement covariance matrix was taken to be diagonal  $\mathbf{S}_e = \sigma_e^2 \mathbf{I}$ , with  $\sigma_e = 2.5 \times 10^{-6} \text{ W}/(\text{cm}^2 \cdot \text{sr} \cdot \text{m}^{-1})$ , which is of the order of the RMS of a typical spectral fit (see Fig. 6). The a priori covariance matrix  $\mathbf{S}_a$  was taken as Gaussian (see Barret et al., 2005a). For  $\text{SO}_2$  the diagonal values were chosen to be proportional to the BT difference in the  $\nu_3$  band (this choice will be justified in the next section). For the other molecules they were chosen to be constant and corresponding to a relative standard deviation of 25%. The iteration from Eq. (4) was repeated until

Title Page

Abstract

Introduction

Conclusions

References

Tables

Figures

◀

▶

◀

▶

Back

Close

Full Screen / Esc

Printer-friendly Version

Interactive Discussion



$$|F(\hat{\mathbf{x}}_i) - F(\hat{\mathbf{x}}_{i+1})| < 0.2\sigma_e.$$

### 4.3 Retrieval of the SO<sub>2</sub> profile

#### 4.3.1 Day of the eruption

A typical fit and corresponding vertical profile for spectra on 30 September are shown in Fig. 6 and Fig. 7. Figure 8 summarises the total retrieval, i.e. the brightness temperature difference, the concentration, the DOFS of the SO<sub>2</sub> retrieval and the retrieved height of the concentration peak. The first thing to note is the clear correlation between the BT difference and the SO<sub>2</sub> concentration (see in this context also Prata et al., 2003). Figure 9 shows the relation more explicitly. For low concentrations (<30 DU) there is an almost linear correlation between the two, while for higher concentrations the BT difference progressively saturates. This correlation can be derived using simplified versions of Eqs. (1) and (2). Let us assume a layer of SO<sub>2</sub> centred at an altitude of 16.5 km. The radiance at wavenumber  $\nu$  entering the layer can be written as  $B(\nu, T_a)$ , where  $T_a$  is total brightness temperature of the layers below. The radiance leaving the layer can then be written as

$$B(\nu, T_b) = B(\nu, T_a)\tau + B(\nu, T_{165})(1 - \tau),$$

with  $T_{165}=192\text{ K}$  the temperature at 16.5 km according to the tropical model,  $\tau = \exp(-c_1 C)$  the transmittance,  $C$  the SO<sub>2</sub> concentration and  $c_1$  a coefficient dependent on temperature, pressure and thickness of the layer. The BT difference we wish to find is given by  $\Delta BT = T_a - T_b$  (in view of the altitude, we ignore absorption above the SO<sub>2</sub> layer). After straightforward calculus one finds

$$T_b = \frac{A}{\ln[1 + GH/(H\tau + G(1 - \tau))]}, \quad (5)$$

with  $A = h\nu/k$ ,  $G = \exp(A/T_a) - 1$  and  $H = \exp(A/T_{165}) - 1$ . From Eq. (5) one can see that when the concentration is very large the observed temperature  $T_b$  approaches

16928

Title Page

Abstract

Introduction

Conclusions

References

Tables

Figures

◀

▶

◀

▶

Back

Close

Full Screen / Esc

Printer-friendly Version

Interactive Discussion



**Tracking volcanic  
SO<sub>2</sub> with IASI**

L. Clarisse et al.

[Title Page](#)[Abstract](#)[Introduction](#)[Conclusions](#)[References](#)[Tables](#)[Figures](#)[◀](#)[▶](#)[◀](#)[▶](#)[Back](#)[Close](#)[Full Screen / Esc](#)[Printer-friendly Version](#)[Interactive Discussion](#)

$T_{165}$ . This again shows the importance of thermal contrasts between  $T_a$  and  $T_b$  as  $\Delta BT$  is effectively bounded by  $T_a - T_b$ . Using linear squares regression, we found values of  $T_a = 243$  K and  $c_1 = 0.034$  DU<sup>-1</sup>. The resulting curve (Fig. 9) matches the data very well. Note that the a priori variability (covariance matrix) for the SO<sub>2</sub> retrievals was chosen proportional to the BT difference. The non-linear correlation between the concentration and the BT difference indicates that the retrievals were not affected by this choice. We verified on a sample of spectra that – as long as it was chosen large enough, the retrieved concentration is pretty much independent of the variability.

The DOFS graph in Fig. 8 shows a moderate correlation with the SO<sub>2</sub> concentration. The maximum DOFS is around 2.3; and with a retrieval between 12 and 21 km this corresponds to a vertical resolution smaller than 4 km. It also shows that three partial columns is the right choice for the retrievals for the first day of the eruption. Fewer columns would mean disregarding available information, while more partial columns lead to erratic profiles because of the necessarily large diagonal of the a priori covariance matrix  $\mathbf{S}_a$ . Another good indication is that for almost all retrieved pixels, the peak of the averaging kernel is the same as the corresponding retrieval level (i.e. the information on a partial column comes primarily from the right altitude). The altitudes where the SO<sub>2</sub> concentration reaches its peak in the profile is typically between 14 km and 17 km. The highest concentrations all had a peak altitude of about 16.5 km. This result is in excellent agreement with information from other satellites and atmospheric transport model simulations (Eckhardt et al., 2008).

### 4.3.2 Tracking the plume

As shown in Fig. 2, IASI was able to follow the plume for almost twelve days. Three partial columns of SO<sub>2</sub> were fitted from the spectra of the first 36 h after the eruption. Retrievals from spectra after that typically had a DOFS of 1 and lower. For this reason, only total columns of SO<sub>2</sub> were retrieved for those. The evolution of the total mass is shown in Fig. 10. It was calculated using the average total column in an area around the observed plume. The first three days after the eruption, the total column peaks

around 46 kt, after which it drops to around and below 10 kt. Eckhardt et al. (2008) estimate the total emitted mass to be of the order of 75 kt, based on measurements of the OMI satellite. A discrepancy of the vertical profile is probably responsible for this difference. Another difference with the retrievals from OMI, AIRS and SEVIRI presented in Eckhardt et al. (2008) is that the evolution of the retrieved mass in our retrieval is much smoother. The retrieved SO<sub>2</sub> mass from OMI shows for instance an increase (from over 60 kt to over 100 kt) from 1 to 3 October, while AIRS shows a sharp decrease (from over 100 kt to less than 60 kt) in the same period.

## 5 Ice

Ice can be a significant component of volcanic eruption clouds (Rose et al., 2004) and can hinder retrieval of volcanic ash as well as play a role in scavenging SO<sub>2</sub> (Textor et al., 2003). Ice nucleation may also be a common occurrence in volcanic clouds due to the seeding potential of volcanic ash particles (Durant et al., 2008). Measurements from the SEVIRI instrument reported by Eckhardt et al. (2008) suggest that ice was present in the Jebel at Tair eruption cloud. This was deduced by differencing top-of-atmosphere brightness temperatures in SEVIRI channels centred near 11 and 12 μm, which are strongly positive for semi-transparent ice clouds (Wu, 1987). The cause of the differences has been determined through radiative transfer theory (Parol et al., 1991) to be due to differential absorption and scattering by ice (spheres and cylinders have been considered), resulting ultimately from differences in the complex refractive indices of ice at the two wavelengths.

If ice particles were present in the Jebel eruption cloud, then in principle they should be detectable in the IASI brightness temperature spectra, especially within the window region between 800–1000 cm<sup>-1</sup>. To investigate whether ice was present, we have performed some discrete ordinates radiative transfer calculations for ice spheres using Mie theory, and coupled this with Modtran-4 radiance calculations for atmospheric absorption using a nearby radiosonde profile. The resulting radiances were converted to

Title Page

Abstract

Introduction

Conclusions

References

Tables

Figures

◀

▶

◀

▶

Back

Close

Full Screen / Esc

Printer-friendly Version

Interactive Discussion



**Tracking volcanic  
SO<sub>2</sub> with IASI**

L. Clarisse et al.

brightness temperatures and compared directly with an IASI spectrum in the eruption cloud. The real and imaginary parts of the refractive index of ice based on the values provided in Warren (1984) for the region 720–1450 cm<sup>-1</sup>, tabulated in wavelength (μm) at resolutions of 0.1 to 0.3 μm (10–30 cm<sup>-1</sup> at 10 μm) were interpolated to the resolution of IASI of 0.25 cm<sup>-1</sup>. There is a peak in the imaginary part of the refractive index near 800 cm<sup>-1</sup> and a decrease either side of this maximum. Thus absorption of infrared radiation would be expected to decrease as the wavenumber increases from 800 cm<sup>-1</sup> to 1000 cm<sup>-1</sup>. The rate of this decrease in absorption depends on ice particle size and optical depth (Huang et al., 2004). To get an idea of the location of the possible ice plume, we have plotted in Fig. 11 the brightness temperature difference of two almost clear channels at 996.25 cm<sup>-1</sup> and 923.75 cm<sup>-1</sup> on 30 September. The location of the ice plume does not exactly coincide with the location of the SO<sub>2</sub> plume, indicating a difference in altitude.

The IASI brightness temperature spectrum of a pixel in the cloud is shown in Fig. 12, together with the radiative transfer simulation. The simulation uses the interpolated refractive indices in a Mie calculation to determine the extinctions coefficients due to scattering and absorption, the phase functions and asymmetry parameters for a range of particle sizes over the wavenumber domain of interest (720–1450 cm<sup>-1</sup>). These parameters are then used in a discrete ordinates radiative transfer program (e.g. Stamnes and Swanson (1981) to calculate the brightness temperature spectra for a plane-parallel cloud of varying optical thickness. In this model all radiative processes occurring above the cloud are ignored and the radiances entering the cloud base are calculated from the Modtran-4 radiative transfer program (see Anderson et al., 1995; Berk et al., 1989) with local radiosonde data as input for the temperature and water vapour profiles, while all other gas and aerosol profiles are fixed at the US Standard Atmosphere values. It is noted that there is a potential error in this model, since it is likely that some aerosol (volcanic ash) may be present in the cloud; however in the absence of data on the ash we are unable to include any effects in the model. The brightness temperature spectra for four different mean effective particle radii for an infrared optical depth of

[Title Page](#)[Abstract](#)[Introduction](#)[Conclusions](#)[References](#)[Tables](#)[Figures](#)[◀](#)[▶](#)[◀](#)[▶](#)[Back](#)[Close](#)[Full Screen / Esc](#)[Printer-friendly Version](#)[Interactive Discussion](#)

**Tracking volcanic  
SO<sub>2</sub> with IASI**

L. Clarisse et al.

[Title Page](#)[Abstract](#)[Introduction](#)[Conclusions](#)[References](#)[Tables](#)[Figures](#)[◀](#)[▶](#)[◀](#)[▶](#)[Back](#)[Close](#)[Full Screen / Esc](#)[Printer-friendly Version](#)[Interactive Discussion](#)

0.30 at  $1000\text{ cm}^{-1}$  are shown as coloured lines on Fig. 12. It can be seen that there is a reasonable fit between the simulated spectrum for  $r=26\text{ }\mu\text{m}$  and the IASI spectrum and poorer fits for the other particle sizes. Of particular interest is the region between  $800\text{--}1000\text{ cm}^{-1}$  because this region is an atmospheric “window” and likely to show the strongest response to ice, based on the refractive index variation with wavenumber. Thus, when ice is present the slope of the spectrum between  $800\text{--}1000\text{ cm}^{-1}$  will increase, and will show greatest increase for smallest particle sizes. The IASI spectrum suggests that the ice particles are likely to be at least  $20\text{ }\mu\text{m}$  in radius, but not larger than  $30\text{ }\mu\text{m}$ . The best fit between the simulations and the IASI spectrum is for a particle radius of  $26\text{ }\mu\text{m}$ . The slope appears to be quite sensitive to particle size, a result which agrees with Huang et al. (2004). In particular there is a shoulder in the spectrum within region between  $990\text{--}1000\text{ cm}^{-1}$  that is especially sensitive and affords the opportunity of determining particle size from high spectral resolution infrared data (e.g. IASI and AIRS). The calculations that have been performed assumed spherical ice particles and it is known that particle shape can alter the phase function and hence influence the radiative transfer. Particle shape has not been investigated here and we refer to prior work (Fu et al., 1999), which suggests that by treating non-spherical ice particles as spheres of equivalent projected area or volume, errors of  $\sim 10\%$  may be expected for small particles ( $r < 40\text{ }\mu\text{m}$ ) at wavelengths between  $8\text{--}13\text{ }\mu\text{m}$ . Further research is necessary to investigate whether high resolution infrared spectra can be used to infer ice crystal habit, which may be quite complex in vertically extensive volcanic clouds.

## 6 Conclusions

IASI provides near real time measurements and covers both the  $\nu_1$  and  $\nu_3$  band of  $\text{SO}_2$  with very high spectral resolution. We have made an analysis of IASI’s sensitivity to  $\text{SO}_2$  in both bands, and concluded that in principle  $\text{SO}_2$  can be sensed down to the surface. IASI’s potential in analysing volcanic eruptions was demonstrated with the moderate October eruption at Jebel at Tair as a test-case. Using the brightness

---

**Tracking volcanic  
SO<sub>2</sub> with IASI**L. Clarisse et al.

---

[Title Page](#)[Abstract](#)[Introduction](#)[Conclusions](#)[References](#)[Tables](#)[Figures](#)[◀](#)[▶](#)[◀](#)[▶](#)[Back](#)[Close](#)[Full Screen / Esc](#)[Printer-friendly Version](#)[Interactive Discussion](#)

temperature difference of some well chosen channels in the  $\nu_3$  band as a filter, we were able to track the SO<sub>2</sub> plume for 12 days after the eruption. This filter has been tested on six months of global IASI data and has detected all major eruptions, while yielding no false alerts. It is also computationally straightforward and therefore suitable for real-time applications. Likewise, we have shown that the relative intensities of the absorption lines in the  $\nu_3$  band can be used to give a rough estimate of the plume's altitude. IASI's spectral resolution has allowed us to carry out detailed SO<sub>2</sub> profile retrievals, giving us estimates of the concentration and peak altitude. Moderately coarse vertical profiles were also retrieved. IASI also allows direct detection of ash and ice, sometimes found in eruptions, and the high spectral resolution allows the retrieval of microphysical properties such as particle sizes. A detailed study of aerosol detection with IASI will be the subject of further research.

*Acknowledgements.* IASI has been developed and built under the responsibility of the Centre National d'Etudes Spatiales (CNES, France). It is flown onboard the Metop satellites as part of the EUMETSAT Polar System. The IASI L1 data are received through the EUMETCast near real time data distribution service. L. Clarisse and P. F. Coheur are respectively Scientific Research Worker (Collaborateur Scientifique) and Research Associate (Chercheur Qualifié) with F. R. S.-FNRS. C. Clerboux and J. Hadji-Lazaro are grateful to CNES for scientific collaboration and financial support. The research in Belgium was funded by the F. R. S.-FNRS (M. I. S. n°F.4511.08), the Belgian State Federal Office for Scientific, Technical and Cultural Affairs and the European Space Agency (ESA-Prodex arrangements C90-219). Financial support by the "Actions de Recherche Concertées" (Communauté Française de Belgique) is also acknowledged. The authors would like to thank Jean-Noël Thépaut for providing us with the data of the ECMWF wind fields which were used to produce Fig. 2.

## References

Anderson, G., Kneizys, F., Chetwynd, J., Wang, J., Hoke, M., Rothman, L., Kimball, L. M., McClatchey, R., Shettle, E., Clough, S., Gallery, W., Abreu, L., and Selby, J.: FAS-

- CODE/MODTRAN/LOWTRAN: Past/Present/Future, 18th Annual Review Conference on Atmospheric Transmission Models, 1–16, 1995. 16931
- Andres, R. and Kasgnoc, A.: A time-averaged inventory of subaerial volcanic sulfur emissions, *J. Geophys. Res.*, 103, 25 251–25 261, 1998. 16919
- 5 Barret, B., Hurtmans, D., Carleer, M., Mazière, M. D., Mahieu, E., and Coheur, P.-F.: Line narrowing effect on the retrieval of HF and HCL vertical profiles from ground-based FTIR measurements, *J. Quant. Spectrosc. Ra.*, 95, 499–519, 2005a. 16921, 16925, 16927
- Barret, B., Turquety, S., Hurtmans, D., Clerbaux, C., Hadji-Lazaro, J., Bey, I., Auvray, M., and Coheur, P.-F.: Global carbon monoxide vertical distributions from spaceborne high-resolution
- 10 FTIR nadir measurements, *Atmos. Chem. Phys.*, 5, 2901–2914, 2005b, <http://www.atmos-chem-phys.net/5/2901/2005/>. 16921, 16925
- Berk, A., Bernstein, L., and Robertson, D.: MODTRAN: a moderate resolution model for LOW-TRAN 7., Tech. rep., GL-TR-89-0122, Air Force Geophysics Laboratory, Hanscom AFB., 38 pp., 1989. 16931
- 15 Carn, S., Strow, L., de Souza-Machado, S., Edmonds, Y., and Hannon, S.: Quantifying tropospheric volcanic emissions with AIRS: The 2002 eruption of Mt Etna (Italy), *Geophys. Res. Lett.*, 32, L02301, doi:10.1029/2004GL021034, 2005. 16920
- Clerbaux, C., Hadji-Lazaro, J., Turquety, S., George, M., Coheur, P.-F., Hurtmans, D., Wespes, C., Herbin, H., Blumstein, D., Tournier, B., and Phulpin, T.: The IASI/MetOp I Mission: First observations and highlights of its potential contribution to GMES, *COSPAR Inf. Bul.*, 2007, 19–24, 2007. 16920
- 20 Coheur, P.-F., Barret, B., Turquety, S., Hurtmans, D., Hadji-Lazaro, J., and Clerbaux, C.: Retrieval and characterization of ozone vertical profiles from a thermal infrared nadir sounder, *J. Geophys. Res.*, 110, D24303, doi:10.1029/2005JD005845, 2005. 16921, 16925
- 25 Durant, A., Shaw, R., Rose, W., Y.Mi, and Ernst, G.: Ice nucleation and overseeding of ice in volcanic clouds, *J. Geophys. Res.*, 113, D09206, doi:10.1029/2007JD009064, 2008. 16930
- Eckhardt, S., Prata, A. J., Seibert, P., Stebel, K., and Stohl, A.: Estimation of the vertical profile of sulfur dioxide injection into the atmosphere by a volcanic eruption using satellite column measurements and inverse transport modeling, *Atmos. Chem. Phys.*, 8, 3881–3897, 2008, <http://www.atmos-chem-phys.net/8/3881/2008/>. 16920, 16921, 16929, 16930
- 30 Fu, Q., Sun, W., and Yang, P.: Modeling of scattering and absorption by nonspherical cirrus ice particles at thermal infrared wavelenghts, *J. Atmos. Sci.*, 56, 2937–2947, 1999. 16932
- Halmer, M., Schmincke, H.-U., and Graf, H.-F.: The annual volcanic gas input into the atmosph-

---

**Tracking volcanic  
SO<sub>2</sub> with IASI**L. Clarisse et al.

---

[Title Page](#)[Abstract](#)[Introduction](#)[Conclusions](#)[References](#)[Tables](#)[Figures](#)[◀](#)[▶](#)[◀](#)[▶](#)[Back](#)[Close](#)[Full Screen / Esc](#)[Printer-friendly Version](#)[Interactive Discussion](#)

- pere, in particular into the stratosphere: a global data set for the past 100 years, *J. Volcanol. Geoth. Res.*, 115, 511–528, 2002. 16918
- Huang, H.-L., Yang, P., Wei, H., Baum, B., Hu, Y., Antonelli, P., and Ackerman, S.: Inference of ice cloud properties from high spectral resolution infrared observations, *IEEE T. Geosci. Remote Sens.*, 42, 842–853, 2004. 16931, 16932
- 5 Krueger, A., Walter, L., Bhartia, P., Schnetzler, C., Krotkov, N., Sprod, I., and Bluth, G.: Volcanic sulfur dioxide measurements from the Total Ozone Mapping Spectrometer (TOMS) Instruments., *J. Geophys. Res.*, 100, 14 057–14 076, 1995. 16919
- Lee, C., Richter, A., Lee, H., Kim, Y., Burrows, J., Lee, Y., and Choi, B.: Impact of transport of sulfur dioxide from the Asian continent on the air quality over Korea during May 2005, *Atmos. Environ.*, 42, 1461–1475, 2008. 16919
- 10 Li, J., Li, J., Weisz, E., and Zhou, D.: Physical retrieval of surface emissivity spectrum from hyperspectral infrared radiances, *Geophys. Res. Lett.*, 34, L16812, doi:10.1029/2007GL030543, 2007. 16927
- 15 Loyola, D., van Geffen, J., Valks, P., Erbetseder, T., Roozendaal, M. V., Thomas, W., Zimmer, W., and Wißkirchen, K.: Satellite-based detection of volcanic sulphur dioxide from recent eruptions in Central and South America, *Adv. Geosci.*, 14, 35–40, 2008, <http://www.adv-geosci.net/14/35/2008/>. 16919
- Mlawer, E., Clough, S., and Tobin, D.: The MT\_CKD water vapor continuum: a revised perspective including collision induced effects, presented at the Atmospheric Science from Space using Fourier Transform Spectrometry (ASSFTS) Workshop, Bad Wildbad, Germany., [http://www-imk.fzk.de/asf/ame/ClosedProjects/assfts/O.I.7.Clough\\_SA.pdf](http://www-imk.fzk.de/asf/ame/ClosedProjects/assfts/O.I.7.Clough_SA.pdf), 2003. 16922
- 20 Parol, F., Buriez, J., Brogniez, G., and Fouquart, Y.: Information content of AVHRR channels 4 and 5 with respect to the effective radius of cirrus cloud particles, *J. Appl. Meteorol.*, 30, 973–984, 1991. 16930
- 25 Phulpin, T., Blumstein, D., Prel, F., Tournier, B., Prunet, P., and Schlüssel, P.: Applications of IASI on MetOp-A: first results and illustration of potential use for meteorology, climate monitoring, and atmospheric chemistry, *Proc. SPIE*, 6684, 66840F, doi:10.1117/12.736816, 2007. 16920
- 30 Prata, A. and Bernardo, C.: Retrieval of volcanic SO<sub>2</sub> column abundance from Atmospheric Infrared Sounder data, *J. Geophys. Res.*, 112, D20204, doi:10.1029/2006JD007955, 2007. 16923, 16924
- Prata, A. and Kerkmann, J.: Simultaneous retrieval of volcanic ash and SO<sub>2</sub> using MSG-SEVIRI

---

**Tracking volcanic  
SO<sub>2</sub> with IASI**L. Clarisse et al.

---

Title Page

Abstract

Introduction

Conclusions

References

Tables

Figures

◀

▶

◀

▶

Back

Close

Full Screen / Esc

Printer-friendly Version

Interactive Discussion



measurements, *Geophys. Res. Lett.*, 34, L05813, doi:10.1029/2006GL028691, 2007. 16919

Prata, A., Rose, W., Self, S., and O'Brien, D. M.: Global, long-term sulphur dioxide measurements from TOVS data: A new tool for studying explosive volcanism and climate, in: *Volcanism and the Earth's Atmosphere*, edited by: Robock, A. and Oppenheimer, C., 139, *Geophys. Monogr.*, 75–92, AGU, Washington, D.C., 2003. 16928

Robock, A.: Volcanic eruptions and climate., *Rev. Geophys.*, 38, 191–219, 2000. 16919

Rodgers, C.: Inverse methods for atmospheric sounding: theory and practice, series on atmospheric, oceanic and planetary physics, 2, World Scientific, 240 pp., 2000. 16921, 16925

Rose, W. I., Bluth, G., and Watson, I.: Ice in volcanic clouds: When and where?, in: *Proc. of the 2nd Int. Conf. on Volcanic Ash and Aviation Safety, OFCM, Washington, D.C., Session 3*, 61, Extended observations of volcanic SO<sub>2</sub> and sulfate aerosol in the stratosphere, 2004. 16930

Rothman, L., Jacquemart, D., Barbe, A., Benner, D. C., Birk, M., Brown, L., Carleer, M., Jr., C. C., Chance, K., Coudert, L., Dana, V., Devi, V., Flaud, J.-M., Gamache, R., Goldman, A., Hartmann, J.-M., Jucks, K., Maki, A., Mandin, J.-Y., Massie, S., Orphal, J., Perrin, A., Rinsland, C., Smith, M., Tennyson, J., Tolchenov, R., Toth, R., Auwera, J. V., Varanasi, P., and Wagner, G.: The HITRAN 2004 molecular spectroscopic database, *J. Quant. Spectrosc. Ra.*, 96, 139–204, 2005. 16922

Stamnes, K. and Swanson, R.: A new look at the discrete ordinate method for radiative transfer calculations in anisotropically scattering atmospheres, *J. Atmos. Sci.*, 38, 387–399, 1981. 16931

Stunder, B. J. B., Heffter, J. L., and Draxler, R. R.: Airborne volcanic ash forecast area reliability, *Weather Forecast*, 22, 1132–1139, 2007. 16919

Textor, C., H.-F. Graf, H.-F., and Herzog, M.: Injection of gases into the stratosphere by explosive eruptions, *J. Geophys. Res.*, 108, 4606, doi:10.1029/2002JD002987, 2003. 16930

Watson, I., Realmuto, V., Rose, W., Prata, A., Bluth, G., Gu, Y., Bader, C., and Yu, T.: Thermal infrared remote sensing of volcanic emissions using the moderate resolution imaging spectroradiometer, *J. Volcanol. Geoth. Res.*, 135, 75–89, 2004. 16919

Wen, S. and Rose, W. I.: Retrieval of sizes and total mass of particles in volcanic clouds using AVHRR bands 4 and 5, *J. Geophys. Res.*, 99, 5421–5431, 1994. 16920

Wu, M. C.: A method for remote sensing emissivity, fractional cloud cover, and effective cloud temperature of high-level thin clouds, *J. Clim. Appl. Meteorol.*, 26, 225–233, 1987. 16930

Yang, K., Krotkov, N., Krueger, A., Carn, S., Bhartia, P., and Levelt, P.: Retrieval of large volcanic

**Tracking volcanic  
SO<sub>2</sub> with IASI**

L. Clarisse et al.

Title Page

Abstract

Introduction

Conclusions

References

Tables

Figures

◀

▶

◀

▶

Back

Close

Full Screen / Esc

Printer-friendly Version

Interactive Discussion



---

**Tracking volcanic  
SO<sub>2</sub> with IASI**

L. Clarisse et al.

---

Title Page

Abstract

Introduction

Conclusions

References

Tables

Figures

⏪

⏩

◀

▶

Back

Close

Full Screen / Esc

Printer-friendly Version

Interactive Discussion



Tracking volcanic  
SO<sub>2</sub> with IASI

L. Clarisse et al.

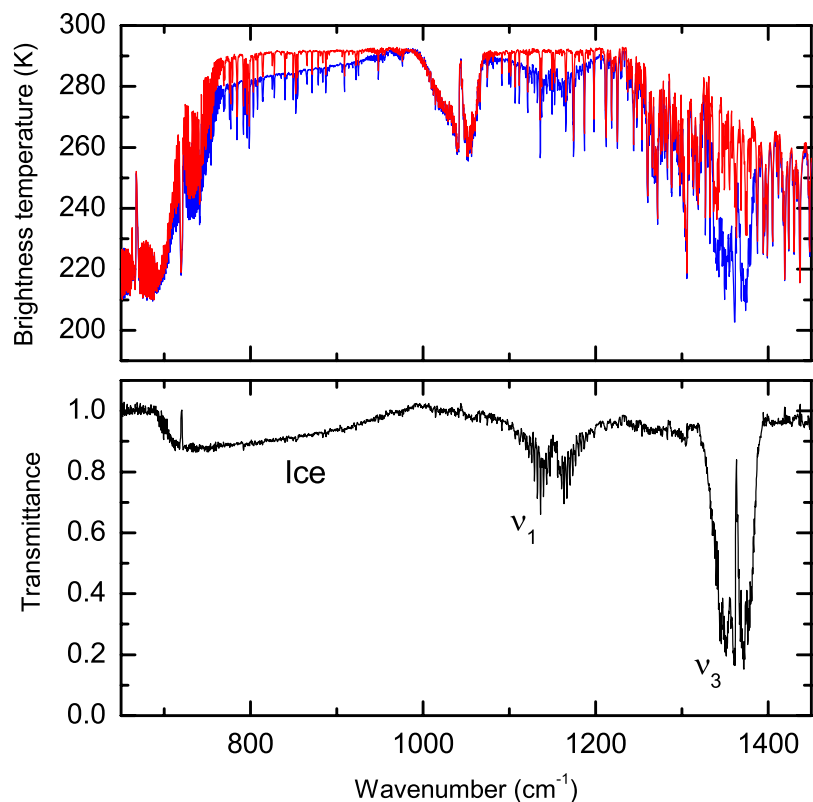


**Fig. 1.** Top panel. Two spectra (in brightness temperature) from 30 September 2007. The spectrum in blue is taken from inside the initial plume of the Jebel at Tair eruption, the spectrum in red is from a nearby pixel, just outside the plume. Bottom panel. Ratio of the two spectra from the top panel.

[Title Page](#)[Abstract](#)[Introduction](#)[Conclusions](#)[References](#)[Tables](#)[Figures](#)[◀](#)[▶](#)[◀](#)[▶](#)[Back](#)[Close](#)[Full Screen / Esc](#)[Printer-friendly Version](#)[Interactive Discussion](#)

Tracking volcanic  
SO<sub>2</sub> with IASI

L. Clarisse et al.

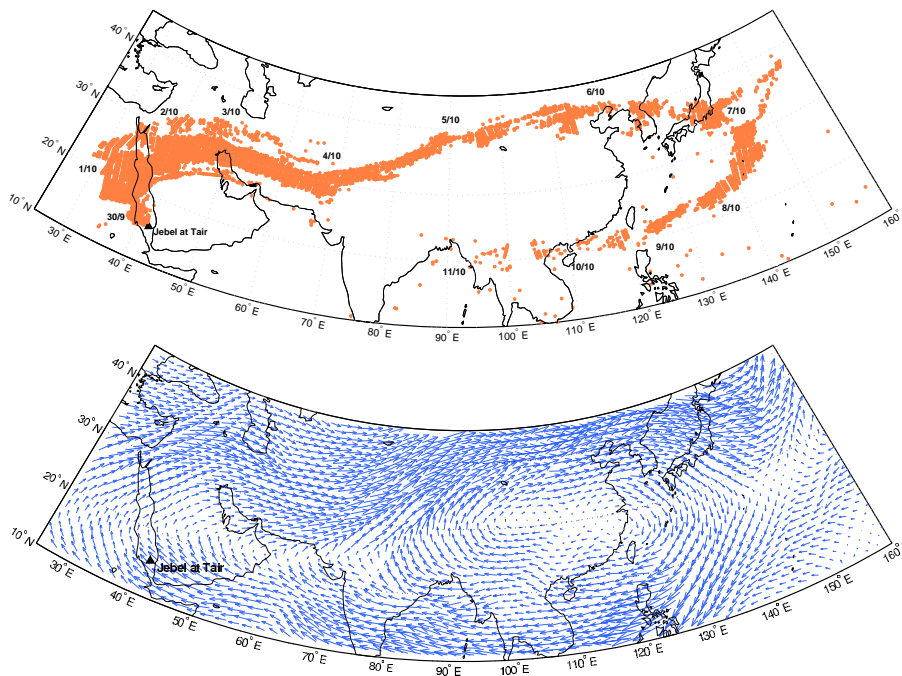


**Fig. 2.** Top panel. Integrated view of the SO<sub>2</sub> plume after the Jebel at Tair eruption on 30 September 2007. The brightness temperature difference in the  $\nu_3$  band was used as a tracker (see Section 3.2). The coloured dots represent retrieved spectra with a brightness temperature difference larger than 0.5 K. Bottom panel. Wind fields at 100 hPa on 6 October (data from the ECMWF, the European Center for Medium range Weather Forecasting).

[Title Page](#)[Abstract](#)[Introduction](#)[Conclusions](#)[References](#)[Tables](#)[Figures](#)[◀](#)[▶](#)[◀](#)[▶](#)[Back](#)[Close](#)[Full Screen / Esc](#)[Printer-friendly Version](#)[Interactive Discussion](#)

Tracking volcanic  
SO<sub>2</sub> with IASI

L. Clarisse et al.

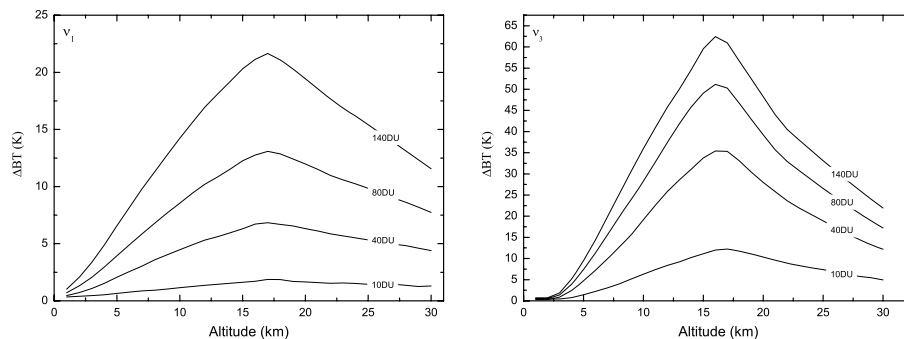


**Fig. 3.** Brightness temperature differences between the baseline and the average brightness temperature of the three strongest IASI channels of the  $\nu_1$  (left) and the  $\nu_3$  (right) band as a function of the altitude and concentration of the SO<sub>2</sub> plume.

[Title Page](#)[Abstract](#)[Introduction](#)[Conclusions](#)[References](#)[Tables](#)[Figures](#)[◀](#)[▶](#)[◀](#)[▶](#)[Back](#)[Close](#)[Full Screen / Esc](#)[Printer-friendly Version](#)[Interactive Discussion](#)

Tracking volcanic  
SO<sub>2</sub> with IASI

L. Clarisse et al.

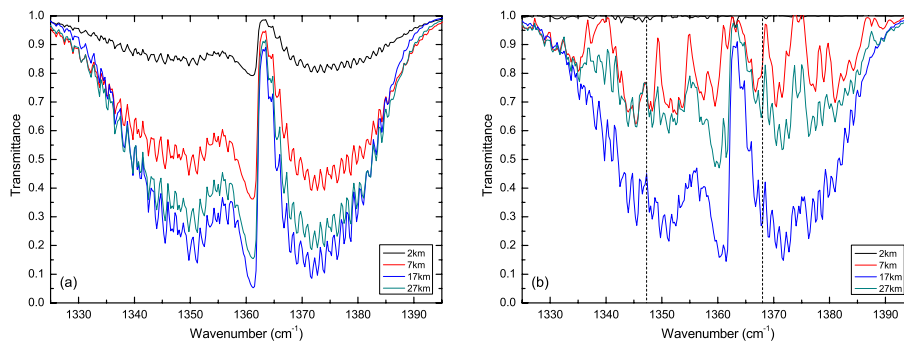


**Fig. 4.** Simulated IASI-like pseudo transmittance spectra of an atmosphere containing (a) only 100 DU SO<sub>2</sub> and (b) 100 DU SO<sub>2</sub> and the 28 first HITRAN molecules at a standard tropical concentration.

[Title Page](#)[Abstract](#)[Introduction](#)[Conclusions](#)[References](#)[Tables](#)[Figures](#)[◀](#)[▶](#)[◀](#)[▶](#)[Back](#)[Close](#)[Full Screen / Esc](#)[Printer-friendly Version](#)[Interactive Discussion](#)

Tracking volcanic  
SO<sub>2</sub> with IASI

L. Clarisse et al.

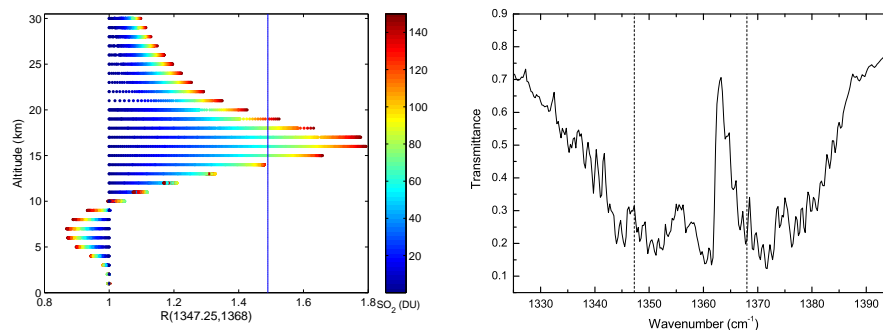


**Fig. 5.** Intensity ratio  $R(1347.25, 1368.00)$  as a function of altitude and concentration. The pseudo transmittance spectrum shown on the right was obtained from an IASI radiance spectrum on 30 September, corresponding to a brightness temperature difference 50 K, divided by a nearby spectrum outside the volcanic plume.

[Title Page](#)[Abstract](#)[Introduction](#)[Conclusions](#)[References](#)[Tables](#)[Figures](#)[◀](#)[▶](#)[◀](#)[▶](#)[Back](#)[Close](#)[Full Screen / Esc](#)[Printer-friendly Version](#)[Interactive Discussion](#)

Tracking volcanic  
SO<sub>2</sub> with IASI

L. Clarisse et al.

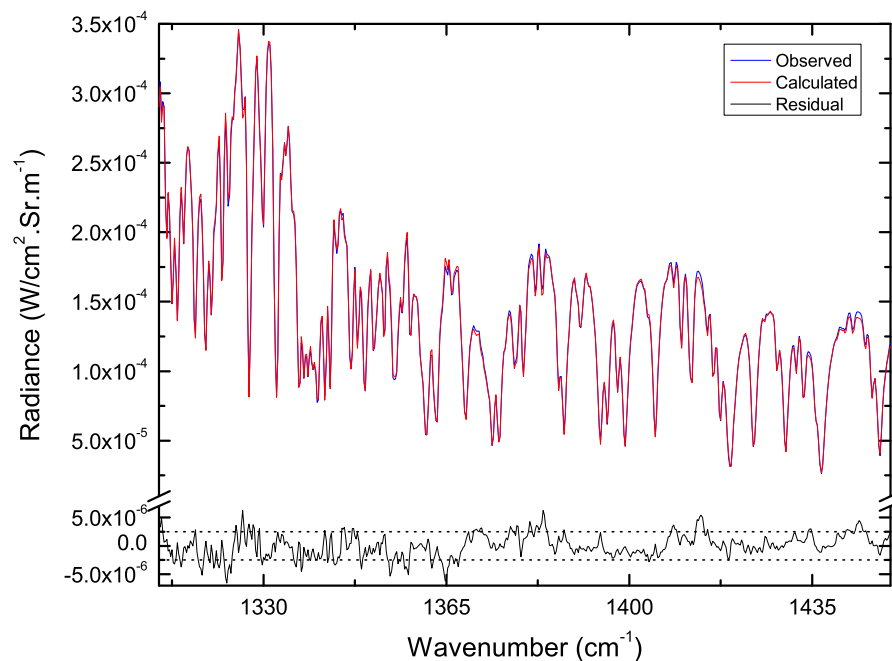


**Fig. 6.** A sample fit of a spectrum from the first day of the eruption. The dotted lines correspond to  $\sigma_\epsilon = \pm 2.5 \times 10^{-6} \text{ W}/(\text{cm}^2 \cdot \text{sr} \cdot \text{m}^{-1})$ .

[Title Page](#)[Abstract](#)[Introduction](#)[Conclusions](#)[References](#)[Tables](#)[Figures](#)[◀](#)[▶](#)[◀](#)[▶](#)[Back](#)[Close](#)[Full Screen / Esc](#)[Printer-friendly Version](#)[Interactive Discussion](#)

**Tracking volcanic  
SO<sub>2</sub> with IASI**

L. Clarisse et al.

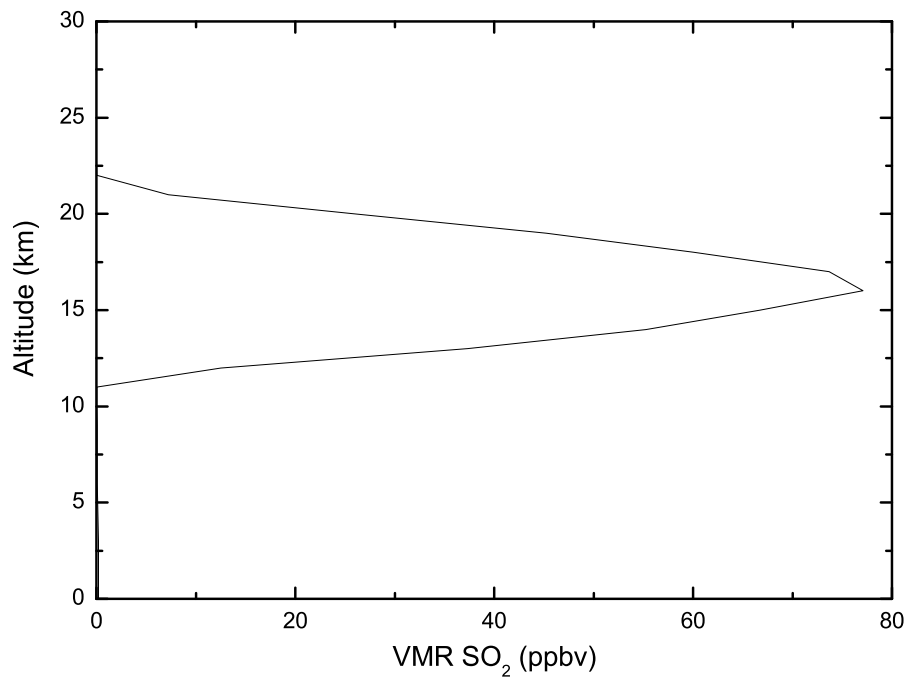


**Fig. 7.** The retrieved vertical profile of SO<sub>2</sub> corresponding to the spectrum displayed in Fig. 5.

[Title Page](#)[Abstract](#)[Introduction](#)[Conclusions](#)[References](#)[Tables](#)[Figures](#)[◀](#)[▶](#)[◀](#)[▶](#)[Back](#)[Close](#)[Full Screen / Esc](#)[Printer-friendly Version](#)[Interactive Discussion](#)

Tracking volcanic  
SO<sub>2</sub> with IASI

L. Clarisse et al.

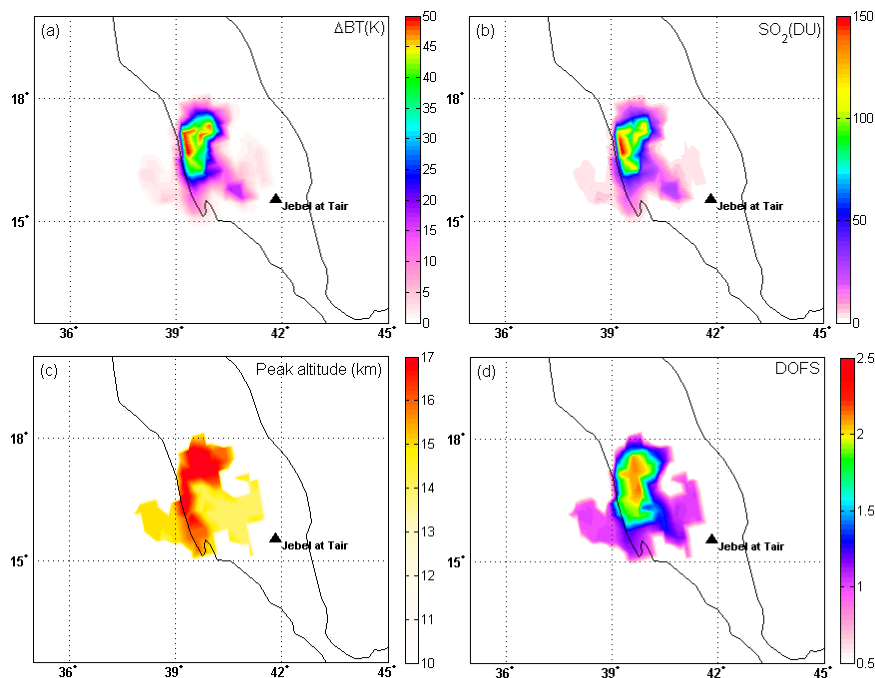


**Fig. 8.** Different views of the volcanic plume from the eruption at Jebel at Tair on 30 September 2007 around 18:48 UTC. **(a)** Brightness temperature differences in the  $\nu_3$  band, **(b)** Retrieved SO<sub>2</sub> concentrations in DU, **(c)** Altitude of peak SO<sub>2</sub> concentration, **(d)** Degrees of freedom for signal.

[Title Page](#)[Abstract](#)[Introduction](#)[Conclusions](#)[References](#)[Tables](#)[Figures](#)[I◀](#)[▶I](#)[◀](#)[▶](#)[Back](#)[Close](#)[Full Screen / Esc](#)[Printer-friendly Version](#)[Interactive Discussion](#)

Tracking volcanic  
SO<sub>2</sub> with IASI

L. Clarisse et al.

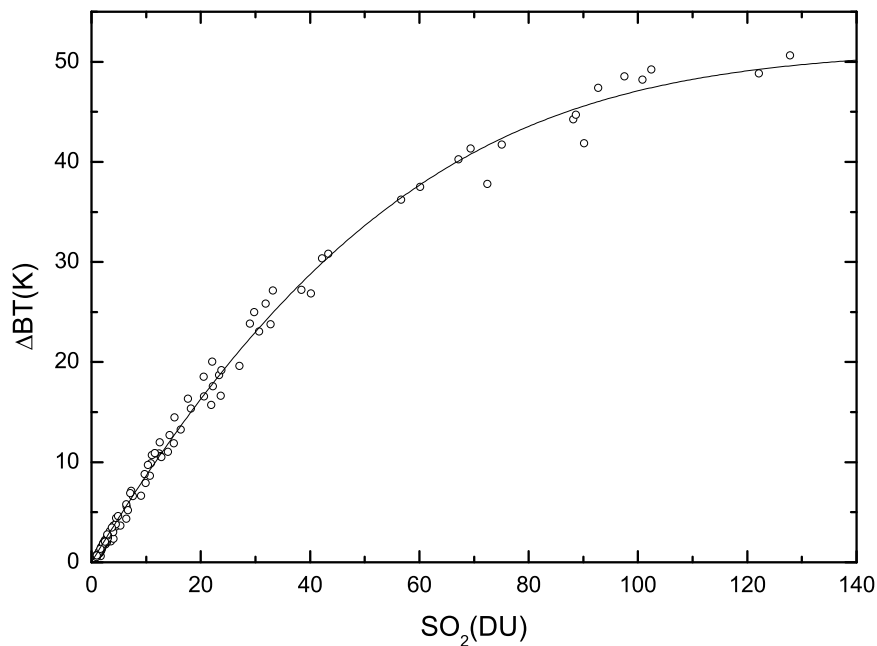


**Fig. 9.** Correlation between the brightness temperature difference and the retrieved SO<sub>2</sub> concentrations. Each circle represents data from one spectrum, the solid line is given by  $\Delta T = T_a - T_b$ , with  $T_b$  given in Eq. (5) with parameters  $T_a = 243$  K and  $c_1 = 0.034$  DU<sup>-1</sup>.

[Title Page](#)[Abstract](#)[Introduction](#)[Conclusions](#)[References](#)[Tables](#)[Figures](#)[◀](#)[▶](#)[◀](#)[▶](#)[Back](#)[Close](#)[Full Screen / Esc](#)[Printer-friendly Version](#)[Interactive Discussion](#)

Tracking volcanic  
SO<sub>2</sub> with IASI

L. Clarisse et al.

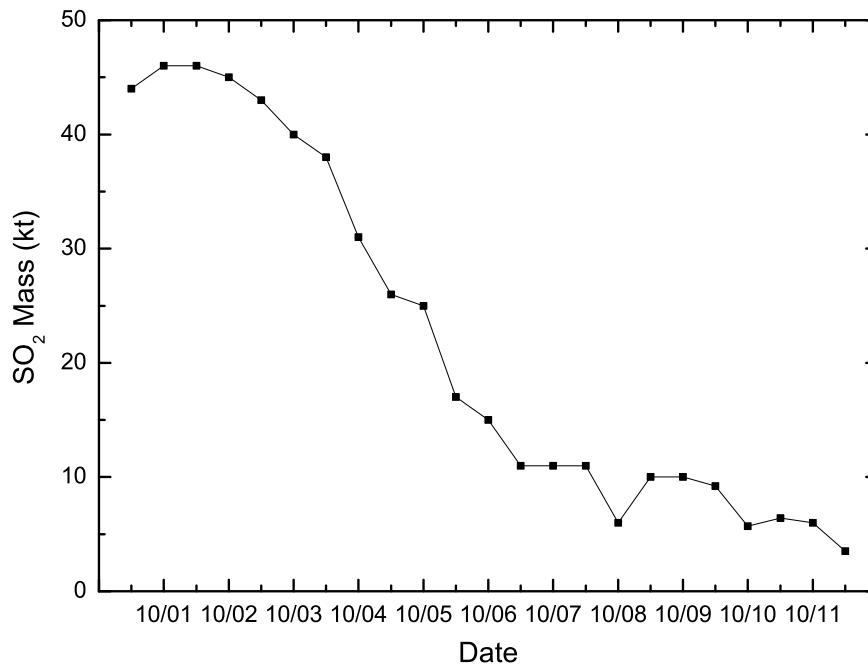


**Fig. 10.** Evolution of the total mass of SO<sub>2</sub> in function of time. Only retrievals with a RMS smaller than  $2\sigma_e$  were retained for the calculation.

[Title Page](#)[Abstract](#)[Introduction](#)[Conclusions](#)[References](#)[Tables](#)[Figures](#)[I◀](#)[▶I](#)[◀](#)[▶](#)[Back](#)[Close](#)[Full Screen / Esc](#)[Printer-friendly Version](#)[Interactive Discussion](#)

Tracking volcanic  
SO<sub>2</sub> with IASI

L. Clarisse et al.

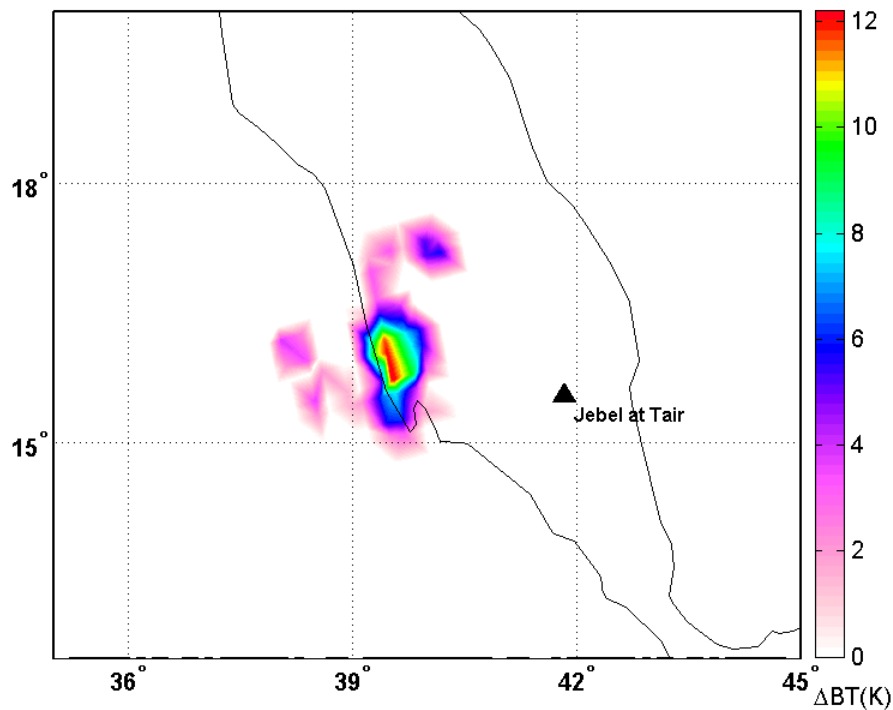


**Fig. 11.** Brightness temperature difference on 30 September 2007 around 18:48 UTC between the channels at  $923.75\text{ cm}^{-1}$  and  $996.25\text{ cm}^{-1}$ , indicating the presence of ice.

[Title Page](#)[Abstract](#)[Introduction](#)[Conclusions](#)[References](#)[Tables](#)[Figures](#)[I◀](#)[▶I](#)[◀](#)[▶](#)[Back](#)[Close](#)[Full Screen / Esc](#)[Printer-friendly Version](#)[Interactive Discussion](#)

Tracking volcanic  
SO<sub>2</sub> with IASI

L. Clarisse et al.

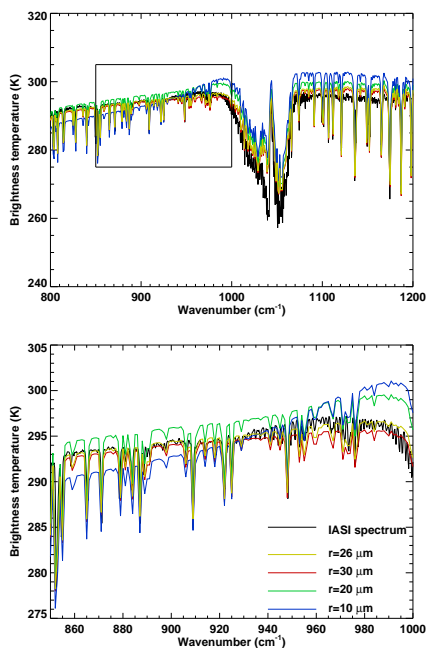


**Fig. 12.** Top panel. Top-of-atmosphere brightness temperature spectra for an IASI measurements (black) and for simulations using a radiative transfer model with four different mean effective spherical ice particle radii, indicated by different colours. Bottom panel. Close-up of the spectra in the region marked by the box, which includes the atmospheric window within which ice effects are expected to be most pronounced. Notice the change in slope of the BT spectra with wavenumber and the sensitivity of the slope to particle size.

[Title Page](#)[Abstract](#)[Introduction](#)[Conclusions](#)[References](#)[Tables](#)[Figures](#)[◀](#)[▶](#)[◀](#)[▶](#)[Back](#)[Close](#)[Full Screen / Esc](#)[Printer-friendly Version](#)[Interactive Discussion](#)